Article

Numerical Simulation Study on the Performance of Buried Pipelines under the Action of Faults

Rulin Zhang [1,*], Chen Wang [1], Shuai Li [1,2], Jixin Zhang [1] and Wenjing Liu [1]

[1] College of Pipeline and Civil Engineering, China University of Petroleum, Changjiang West Road No. 66, Qingdao 266580, China; s19060026@s.upc.edu.cn (C.W.); z20060081@s.upc.edu.cn (S.L.); z22060081@s.upc.edu.cn (J.Z.); z22060077@s.upc.edu.cn (W.L.)
[2] Hebei Branch of China Nuclear Power Engineering Co., Ltd., Shijiazhuang 050019, China
* Correspondence: zhangrulin@upc.edu.cn; Tel.: +86-130-6140-0185

Abstract: The present paper investigates the mechanical behavior of buried steel pipelines crossing an active fault. Permanent ground deformation induced by an earthquake will cause serious damage to buried steel pipelines, resulting in buckling failure or even cracking damage to pipelines. Based on ABAQUS software, version 6.13., the model of an interacting soil–pipeline system is established, accounting for large strains and displacements and nonlinear material behavior, as well as contact and friction at the soil–pipeline interface. Numerical analysis is conducted through the incremental application of fault displacement. Combined with the force and deformation characteristics of buried pipelines, a strain-based design criterion is chosen to study the vertical displacement, axial compressive, and tensile strain of buried pipelines, etc. This paper focuses on the effects of horizontal fault displacement, fault type, and fault angle on the structural response of the pipe. The failure of the pipeline, such as wall wrinkling, local buckling, or rupture is identified. Furthermore, the effects of the pipeline internal pressure and pipe wall thickness are investigated. The results show that, when the pipeline depth is 1.5 m under the action of the fault, the buried pipeline will not be subject to beam buckling damage, and both tensile damage and shell buckling damage will occur. In this case, the critical displacement of the tensile failure is more than three times that of the shell buckling failure, which indicates that shell buckling damage is a greater threat to the pipeline. The pipeline is most susceptible to damage under the action of a strike-slip reverse fault. When the fault angle is equal to 45 degrees, the pipeline is more likely to be damaged, while it is relatively safe at a fault angle with 90 degrees. The results of this investigation can determine the fault displacement during pipeline failure and provide some reference for pipeline design.

Keywords: buried pipeline; fault displacement; buckling; failure mode; finite elements

1. Introduction

Pipeline transportation plays an extremely crucial role in the process of oil and gas extraction, transportation, and deployment due to its high transportation efficiency and better safety. According to post-earthquake surveys, the main reason for serious damage to buried steel pipelines for oil and natural gas is the permanent ground action caused by earthquakes, such as fault movements, landslides, and lateral expansion caused by liquefaction. Permanent ground deformation is applied to the pipeline in a quasi-static manner, which may not necessarily be related to high seismic intensity. However, the pipeline may undergo severe deformation within the plastic range, leading to buckling failure or even cracking damage, posing a significant threat to humans and the environment. Damage to this type of pipeline has been reported in many earthquakes, such as the 1971 San Fernando earthquake [1], the 1995 Kobe earthquake [2], the 1999 Kocaeli earthquake [3], and the 1999 Chi-Chi earthquake [4]. Due to the high degree of overlap between the area through which pipelines must pass and the distribution area of active fault zones, the service life of oil and gas pipelines has suffered from the serious threat of active faults in China [5].

In order to ensure the safety of buried pipelines during permanent strike-slip fault movement, the corresponding deformation and stress state of pipelines should be evaluated. The first researchers to study the response of pipelines under fault displacement were Newmark and Hall [6]; this study used a simplified analytical model of a long cable to calculate stresses and strains within its walls. Guo et al. [7] used the finite element method to solve the response of pipelines and soil under the action of faults in a simple and convenient way. Mitsuya et al. [8] proposed a method for evaluating the seismic performance of buried pipelines to estimate the deformation of pipelines induced by ground deformation of pipelines caused by motion, which can provide a good assessment of pipelines in general. Zhang et al. [9] proposed a finite element model for analyzing the response of a pipeline under a strike-slip fault, and investigated the effects of fault displacement, dynamic friction coefficient, and other factors on the displacement and strain of the pipeline. Using the continuum modelling approach, Banushi et al. [10] presented a parametric analysis of a buried pipeline crossing a strike-slip fault. The proposed modelling procedure can be suitably used to accurately and efficiently analyze the seismic performance of buried pipelines subjected to a similar PGD. Shakib et al. [11] conducted an evaluation of the strain response of buried pipelines under an oblique-slip fault. However, the specific boundary conditions and movement characteristics of the oblique-slip fault movement were not given.

The behavior of buried steel pipelines subjected to a crossing angle has received significant attention. Vazouras et al. [12–14] investigated the mechanical behavior of buried pipelines under the action of strike-slip faults, and derived the critical fault displacements for different damage modes. Assuming that the pipeline passes through the fault plane at different angles, the effects of the crossing angle for several soil and pipe parameters are investigated. In most cases which were analyzed, it is indicated that local buckling is the governing mode of failure for non-positive values of the crossing angle β. For pipelines under tension (positive values of β), local buckling does not dominate. As the angle increases, local buckling caused by longitudinal stretching can be avoided, but the pipeline may fail due to excessive axial tensile strain or a flattened cross-section. Gu and Zhang [15] used numerical methodology, aiming to determine the optimum crossing angle for a pipeline. Cheng et al. [16] made a parametric study on the strain response of an X80 steel pipeline crossing an oblique-slip fault. However, the proposed oblique-slip fault was limited to a strike-slip movement with a fault dip angle of 90 degrees. Cheng et al. [17,18] investigated different failure modes of pipelines under the action of oblique reverse faults by means of a three-dimensional multiple nonlinear finite element model and fitted equations for predicting the range of the local buckling failure of buried pipelines. The failure characteristics and failure range of the local buckling of a buried pipeline were systematically analyzed, and the influence of the fault dip angle, displacement, diameter-thickness ratio, burial depth, and internal pressure on the local buckling failure range of the pipeline was discussed in detail. Apart from the numerical studies, Ha et al. [19,20] and Abdoun et al. [21] also conducted experimental studies on the impact of strike-slip faults on buried polyethylene pipelines. Based on centrifugal modeling, this study investigated the influence of fault types and strike slip fault angles on the mechanical behavior of pipelines, as well as the effects of the embedment depth and pipe diameter.

The present paper extends the work presented in [22], considering buried steel pipelines crossing the fault plane at various angles. Furthermore, this paper examines the mechanical behavior of buried steel pipelines under different fault types, as well as the internal pressure and the wall thickness. In this study, the pipeline–soil interaction model is established under fault action through ABAQUS software, version 6.13., the force and deformation characteristics of the pipeline under fault action are combined, and the strain-based design criterion is selected to analyze the response of the pipeline. The vertical displacement, axial compressive strain, and axial tensile strain of the pipeline under the action of a strike-slip reverse fault are analyzed, and the influence of the fault angle, fault type, internal pressure, and wall thickness on the performance of the pipeline are also

studied. The results of this investigation can determine the fault displacement during pipeline failure and provide some reference for pipeline design.

2. Finite Element Model of Pipe–Soil System

In this study, the structural response of pipelines under fault movement is examined numerically using the finite element program ABAQUS [23]. Considering the nonlinear geometric shapes of soil and pipelines, the mechanical behavior of steel pipes, the surrounding soil, and their interactions is rigorously simulated by describing the large strain of the pipeline soil system and the inelastic material behavior of the pipeline and soil.

2.1. Establishment of the Model

In ABAQUS software, version 6.13., the eight-node linear hexahedral solid element C3D8R and the four-node curved shell element S4R are selected to simulate the soil media around the pipe and the buried pipe, respectively. Referring to the research on the effective calculation length of a pipeline model and the code [24], for the calculation of buried pipelines across faults with equivalent boundaries, large deformation segments near the fault and the length of pipelines not less than 60 times the diameter of the pipeline should be analyzed. According to such regulations, the dimensions of the calculation model in the X, Y, and Z directions are taken as 12 times, 8 times, and 65 times the diameter of the pipe, respectively. The whole finite element model of the soil–pipeline system mainly includes three parts: fixed disk, movable disk, and buried pipeline (as shown in Figure 1).
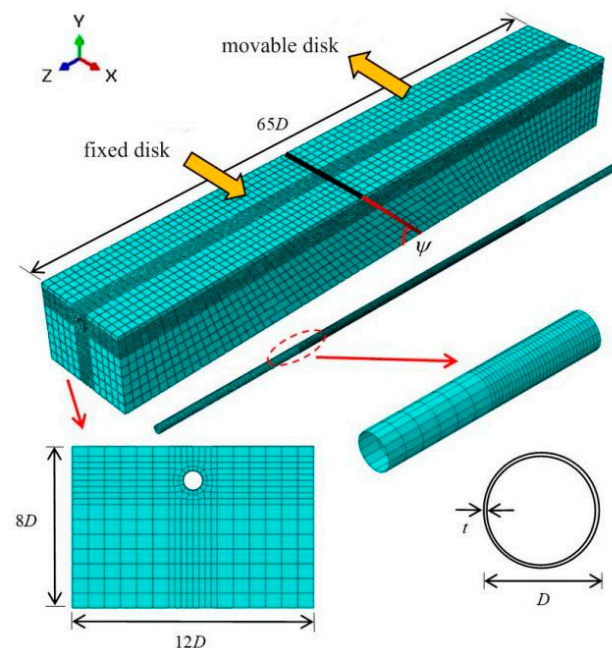
Figure 1. Finite element model of soil–pipeline system.

The focus of this study is to analyze the behavior of the buried pipeline under the action of faults. Taking into account the calculation accuracy, efficiency, and convergence, a more refined mesh division is carried out on the soil within 3 m around the pipeline and its surroundings, as shown in Figure 1. When determining the grid size of the calculation model, the authors referred to the suggestions in the relevant literature and achieved good calculation accuracy. According to the relevant studies [25,26], the pipeline axis direction in the large deformation section is 20 m on both sides of the fault within the range of the pipeline mesh size, which is set to 0.1 m so as to accurately simulate the large deformation characteristics of pipelines, and the grid size of other pipe sections is set to 0.5 m, as shown in Figure 1.

A nonlinear contact model is used to simulate the interaction between the pipeline and soil, as well as between the soil on both sides of the faults. Since the stiffness of pipeline steel is significantly larger than that of soil media, the outer surface of the pipeline is set as the master surface of the contact pair, and the inner surface of the soil is set as the slave surface of the contact pair. The normal action between the contact surfaces is set as "hard" contact, so as to realize the simulation of extrusion on the contact surface between the pipeline and the soil. The tangential action is set as a "penalty" friction function, and the friction coefficient is defined to simulate the shear stresses between the pipeline and the soil in the process of fault misalignment. The shear stress between the pipe and the soil during fault misalignment is simulated by defining the friction factor. In addition, in order to simulate the behavior that the pipe and the soil separate from each other due to excessive relative displacement during the fault movement, the two parts are allowed to separate from each other after contact. Through this setting, the behavior between the pipeline and soil is made to be closer to the actual situation.

This study conducts numerical analysis of the above-established model through the incremental application of fault displacement. The numerical calculation process includes the following three steps. Firstly, gravity loading is applied to the whole model to simulate the initial stress state of the soil in the actual situation. Secondly, an internal operating pressure is applied to the inner wall of the pipeline to simulate the buried gas pipeline under the normal operation state in the actual project. Finally, the fault movable disk is subjected to linear displacement loading.

2.2. Selection of Material Constitutive Model

The classical Mohr–Coulomb yield criterion is used to describe the soil media around the pipeline. Due to the long distance and large span of the buried pipeline, there may be differences in the properties of the soil around the pipeline in both the horizontal and vertical directions. It is difficult to accurately simulate the properties of soil, and this study simplifies it appropriately without considering the spatial changes in soil properties [27]. The relevant parameters of the soil around the pipe are listed in Table 1.

Table 1. Parameters of the soil around the pipeline.

Soil Density/(kg·m^{-3})	Modulus of Elasticity/MPa	Poisson's Ratio	Cohesion/kPa	Friction Angle/Degrees	Shear Angle/Degrees
1900	33	0.3	35	22	0

When the pipe undergoes the action of active fault dislocation, it has to withstand not only the small deformation caused by the internal pressure of normal operation of the pipeline, but also the large deformation generated by the action of fault dislocation, so pipe with a good deformation performance should be used. In this study, the large-deformation pipeline steel pipe X80HD2 is chosen as the research object, and the relevant parameters are mainly obtained from the relevant standards and specifications [28], as shown in Table 2 below.

Table 2. Stress–strain data of X80HD2 steel.

Nominal Stress/MPa	Nominal Strain	True Stress/MPa	True Strain	Plastic Strain
—	—	552	—	0
560	0.00887076	565	0.008831646	0.006102334
580	0.01396761	588	0.013870962	0.011029893
600	0.02272401	614	0.022469666	0.019505248
610	0.02917871	628	0.028761115	0.02572827
620	0.03754717	643	0.036859437	0.033751808
630	0.04835569	660	0.047222927	0.044032279

Table 2. *Cont.*

Nominal Stress/MPa	Nominal Strain	True Stress/MPa	True Strain	Plastic Strain
640	0.06226321	680	0.060401736	0.057117444
650	0.08009188	702	0.077046112	0.073654519
660	0.1028639	728	0.097910342	0.094393964

2.3. Determination of Boundary Conditions

In actual engineering, long-distance pipelines are usually buried in the ground below 0.8~2.5 m, which can be approximated as a semi-infinite domain. By removing a sufficiently large amount of soil including pipelines from the semi-infinite domain and applying reasonable boundary conditions that comply with actual engineering geological conditions, the true working state of buried pipelines can be simulated more realistically. Based on the above premises, this study imposes boundary conditions on the finite element model as shown in Figure 2.

(1) Assuming that the soil on both sides of the fault is in direct contact along the fault displacement surface, without considering the existence of the fault displacement zone, the mutual friction between the soil on both sides is considered through the definition of mutual contact as mentioned earlier, without imposing additional constraints;

(2) No constraints are imposed on the surface of the soil on both sides of the fault to simulate the free ground in actual engineering;

(3) Before applying displacement loads, fixed constraints are applied to the bottom of the soil on both sides of the fault, while the lateral displacement of the soil is limited in its normal direction. During the quasi-static analysis process of applying displacement loads, the non-staggered soil maintains the aforementioned constraints, moves the soil to release the constraints, and applies displacement loads to simulate the fault displacement process.

(**a**)   (**b**)
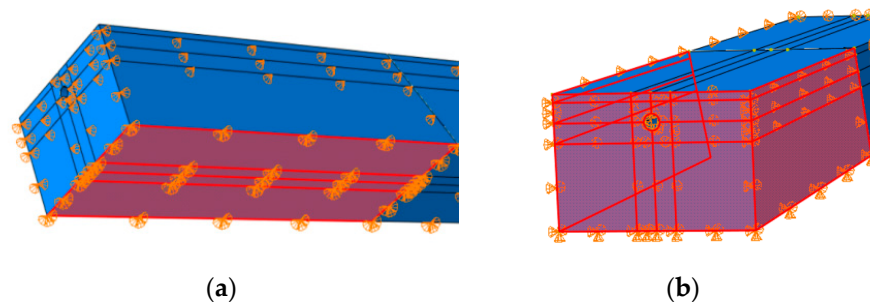
Figure 2. Constraint conditions of soil model: (**a**) At the bottom; (**b**) on the side.

In this study, the fault misalignment displacement δ is estimated by the empirical statistical formula for engineering a design for ground shaking in the Chinese region:

$$\lg\delta = -3.019 + 0.4646 \cdot M, \tag{1}$$

where M is the earthquake magnitude.

According to the distribution of seismic zones along the Second West–East Gas Pipeline Project (China), the minimum magnitude is taken as 4.5 and the maximum magnitude is taken as 7.5, and the fault displacement obtained from the above formula is from 0.12 m to 2.92 m.

3. Analysis of Pipeline Response under the Action of Strike-Slip Reverse Fault

3.1. Analysis of Vertical Displacement Response of Pipeline

The vertical displacement of the pipe under a strike-slip reverse fault is studied to determine whether the damage of the pipeline can be categorized as beam-type buckling. In the model, the burial depth is taken as 1.5 m, the pipe outer diameter is 1.219 m, the wall thickness is 22 mm, the internal pressure is 12 MPa, and the fault angle is 60 degrees. By comparing the vertical displacement of the middle and end of the pipe, it is determined whether it has undergone beam-type buckling failure.

The vertical displacement at the top of the pipe along the pipeline axis under the effect of fault displacement is shown in Figure 3. In Figure 3, δ_{max} indicates the maximum value of vertical displacement of the pipe, and δ_{40} indicates the value of vertical displacement at the end of the pipe on the side of the movable disk. The peak vertical displacement of pipe under different fault displacements is plotted in Table 3.
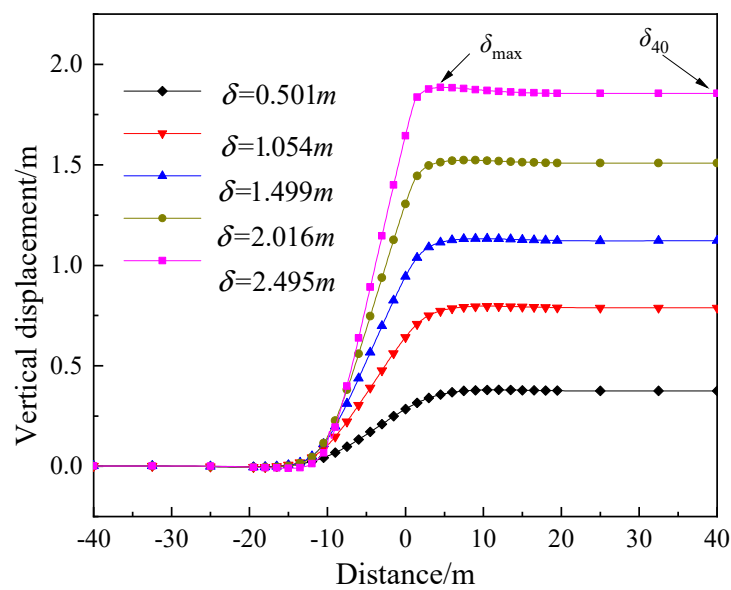
Figure 3. Variation in vertical displacement for different fault displacements.

Table 3. Peak vertical displacement of pipelines for different fault displacements.

Fault Displacement/m	δ_{max}/m	δ_{40}/m	$(\delta_{max} - \delta_{40})$/m	$(\delta_{max} - \delta_{40})/\delta_{max}$
0.501	0.380	0.375	0.005	0.013
1.054	0.797	0.789	0.008	0.010
1.499	1.133	1.122	0.011	0.0097
2.016	1.522	1.508	0.014	0.0092
2.495	1.885	1.868	0.017	0.009

As can be seen from Figure 3, the vertical displacement of the pipe under the action of the fault is basically consistent with the distribution trend along the pipeline axis. From the side of the fixed disk to the side of the movable disk, the response is smooth and unchanged, and then increases rapidly at 10 m away from the fault surface. The maximum displacement occurs at about 4 m away from the fault surface on the side of the movable disk.

From Figure 3, it can be seen that δ_{max} is slightly larger than δ_{40}, which indicates a certain upward bulge in the middle of the pipe. However, as can be seen from Table 3, the difference in vertical displacement of the pipe ($\delta_{max} - \delta_{40}$) is negligible compared to δ_{40} and δ_{max} (both less than 2%), which reflects that there is not a sudden change in vertical displacement along the pipeline axis. That is to say, the pipe in the case of this study does not undergo beam-type buckling damage.

Meyersohn et al. [29] pointed out that the minimum burial depth of the pipe between about 0.5 m and 1.0 m can avoid the occurrence of beam-type buckling damage. Considering both the above results and the relevant codes [24,30,31], the minimum burial depth of the pipe is 0.8 m. In the case of the selected pipe material and the buried depth of 1.5 m in this study, beam-type buckling failure will not occur, which is consistent with the above research conclusion.

3.2. Analysis of Axial Compressive Strain of Pipe

In this section, the axial compressive strain of the pipe is analyzed to determine whether the damage belongs to shell buckling damage or not. This study adopts the critical compressive strain corresponding to the occurrence of pipe-wall shell buckling damage given by CSA Z662-2007 [31] as the basis for judgment:

$$\varepsilon_c^{crit} = 0.5\frac{t}{D} - 0.0025 + 3000\left(\frac{\sigma_h}{E}\right)^2, \tag{2}$$

$$\sigma_h = \begin{cases} \frac{(P_i - P_e)D}{2t} & \frac{(P_i - P_e)D}{2t\sigma_s} < 0.4 \\ 0.4\sigma_s & \frac{(P_i - P_e)D}{2t\sigma_s} \geq 0.4 \end{cases} \tag{3}$$

where ε_c^{crit} is the critical compressive strain at which the pipe undergoes shell buckling damage, t is the thickness of the pipe wall, D is the outer diameter of the pipe, σ_h is the hoop stress, $(P_i - P_e)$ is the internal pressure, and σ_s is the yield stress of the pipe.

Here, D = 1219 mm, t = 22 mm, and $(P_i - P_e)$ = 12 MPa is selected as the object of study. Calculated by the above equations, ε_c^{crit} = 1% is taken as the critical compressive strain for the occurrence of shell buckling damage of the pipe. Taking the case that the pipe crosses a strike-slip reverse fault with an angle 60 degrees, the trend of the maximum compressive strain ε_{cmax} of the pipeline with the displacement of the fault is depicted in Figure 4. The deformation behaviors of the pipe at different stages are shown in Figure 5.

As can be seen from Figure 4, the maximum axial compressive strain increases with the fault displacement, and when the fault displacement is 0.82 m, the maximum axial compressive strain has reached the critical compressive strain of the pipe shell buckling damage. This indicates that the pipeline has started to undergo shell buckling failure at this time.
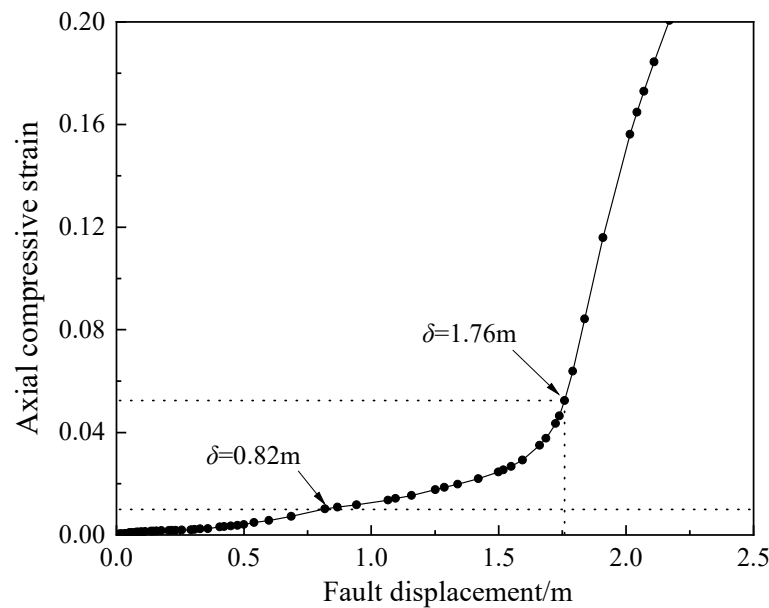
Figure 4. Variation in maximum axial compressive strain under different fault displacements.
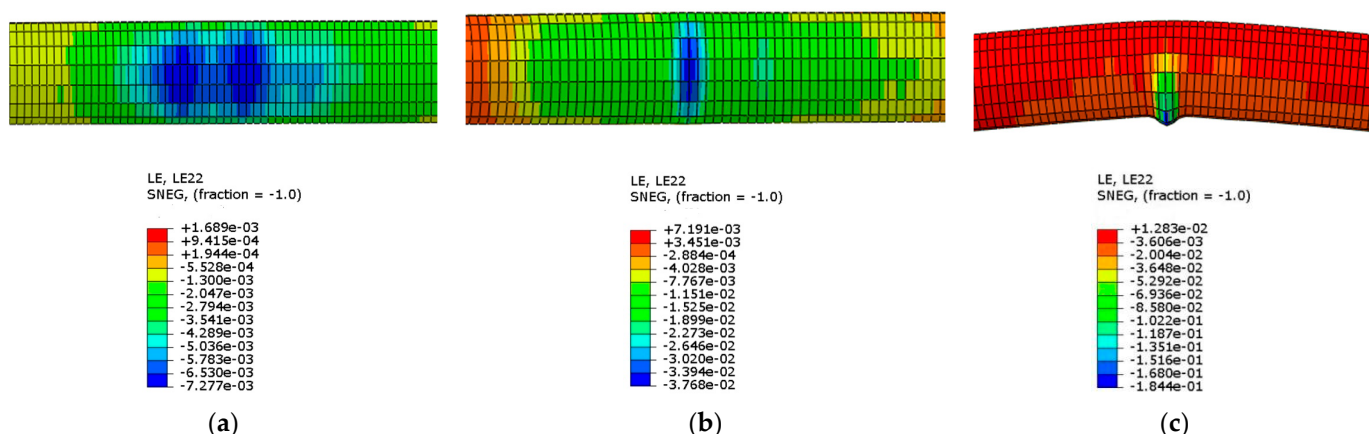
Figure 5. Different stages of local buckling failure of the pipeline: (**a**) Before buckling occurs; (**b**) buckling is expanding; (**c**) tube wall protrusion caused by buckling.

Combined with Figure 5, it can be found that, when the fault displacement is less than 0.82 m (Figure 5a), the pipe wall has not experienced shell buckling damage, and the pipe is still in the elastic stage. As the displacement of the fault increases, small folding and compression deformation gradually begin to appear on the pipe wall. The peak position of axial compressive strain on the pipe wall changes with increasing fault displacement, and at this time, the pipeline does not experience local instability. When the fault displacement is 1.76~0.82 m (Figure 5b), the location of pipe wall has reached the critical compressive strain value. Multiple folds of the pipe wall compressive pattern are gradually concentrated in a certain point, and the maximum axial compressive strain of the pipe wall is also gradually stabilized in the same place. When the fault displacement is more than 1.76 m (Figure 5c), with the increase in the fault displacement, the compressive strain increases rapidly and, under the action of the larger fault displacement and the internal pressure, the pipe wall gradually shows local outward protrusion. At this time, the structural integrity and bearing capacity have been seriously damaged.

3.3. Analysis of Axial Tensile Strain of Pipeline

In this section, the axial tensile strain of the pipe is analyzed to determine whether the damage to the pipe is tensile damage or not. This study refers to the reference value of the ultimate tensile strain specified in [24,31], and takes the ultimate tensile strain of the pipe under the action of the fault as 2.0%.

The maximum tensile strain ε_{tmax} of the pipeline with the increasing displacement of the fault is shown in Figure 6. The tensile strain rises gradually as the displacement of the fault increases. When the fault displacement is 2.72 m, the maximum axial tensile strain reaches the critical tensile strain 2.0%. In accordance with the judgment standard selected as mentioned earlier, the pipeline has already begun to undergo tensile failure.

The displacement of faults is constantly increasing. When the fault displacement is 1.096 m and 1.76 m, the growth rate of ε_{tmax} is slightly increased, and this combined with when the fault displacement is 0.82 m and 1.76 m, it happens to be at the critical point of different stages of shell buckling failure. By comparing the critical damage strain, it can be concluded that the pipe shell buckling damage occurs before the tensile damage. As can be seen in Figure 7, when the fault displacement is up to 1.76 m, it is in the direction of the fault displacement on both sides of the wall, assuming the relative symmetry of ε_{tmax} and ε_{cmax} positions. Therefore, it can be inferred that, when the pipeline undergoes shell buckling failure, it will have a moderate impact on the occurrence of tensile failure.
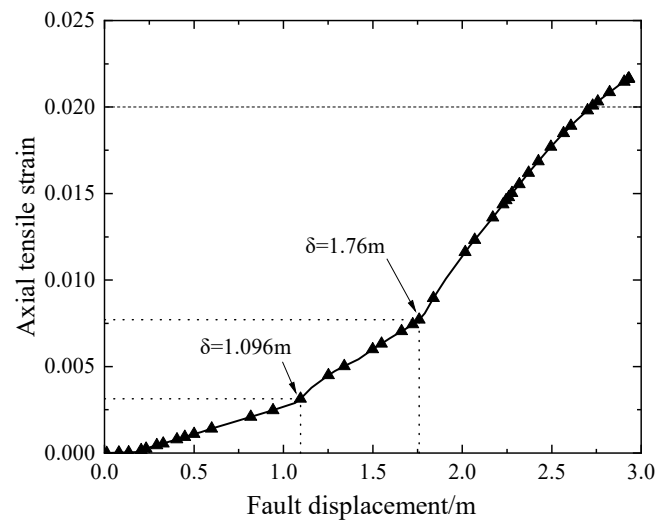
Figure 6. Variation in maximum axial tensile strain under different fault displacements.
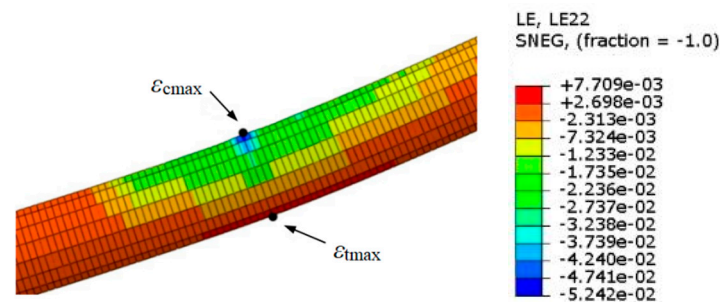
Figure 7. Location of the maximum axial strain when fault displacement is 1.76 m.

In summary, the buried pipeline in this study will not be subject to beam-type buckling damage, while tensile damage and shell buckling damage have occurred in the simulation process, and may cause more serious consequences once they have occurred. Therefore, this study will focus on these two failure modes as the key indicators for pipeline performance evaluation.

4. Analysis of Parameters Affecting Pipeline Response under Fault Action

4.1. Influence of Fault Type

In this part, the pipeline with D = 1219 mm, t = 22 mm, an internal pressure of 12 MPa, and a fault angle of 60 degrees is evaluated, so as to study the influence of different fault types on the performance of the pipe. Figure 8 shows the changes in the maximum axial strain and the maximum von Mises stress with fault displacement under different types of faults.

As shown in Figure 8a, the maximum axial tensile strain rises with the increase in the fault displacement. The growth rate of the axial tensile strain under different types of faults varies, strike-slip fault > strike-slip reverse fault > strike-slip normal fault > reverse fault > normal fault, and the maximum axial tensile strain of the pipe does not reach the critical value of pipeline tensile damage when the displacement of the fault is 2 m.

The situation for the maximum axial compressive strain is different. The growth rate of the axial compressive strain under different types of faults varies as follows, strike-slip reverse fault > reverse fault > strike-slip fault > strike-slip normal fault > normal fault. The growth rates under a strike-slip reverse fault and a reverse fault are obviously larger than others, which indicates that the pipeline suffers from more intense extrusion when the action of a reverse fault exists. When the fault displacement is only 0.82 m, the pipe undergoes shell buckling failure first under the action of a strike-slip reverse fault, and the

positive fault with the slowest growth rate of ε_{cmax} also reaches the critical compressive strain before the fault displacement reaches 2 m.
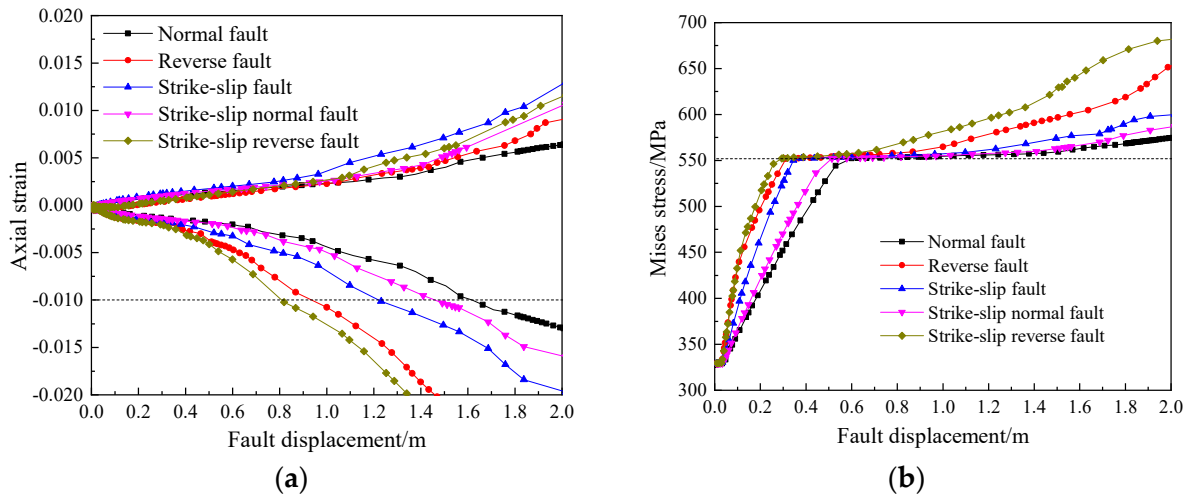
Figure 8. The response of pipeline under different fault types: (**a**) Axial strain; (**b**) von Mises stress.

The variation in the maximum von Mises stress is similar to that of the maximum compressive stress. From Figure 8b, it can be seen that the influence of the fault types on the maximum von Mises stress of the pipe is as follows, strike-slip reverse fault > reverse fault > strike-slip fault > strike-slip normal fault > normal fault, and the stress growth rates under a strike-slip reverse fault, reverse fault, and strike-slip fault are significantly higher than those of a normal fault and strike-slip normal fault before reaching the yield strength.

In summary, in the case of the same fault displacement, the pipeline is more likely to suffer damage when a reverse fault exists. Compared to a single fault type, the combination of strike-slip reverse faults poses greater harm to the buried pipeline. Therefore, in the following research, only strike-slip reverse fault will be addressed.

4.2. Influence of Fault Angle

It can be seen from the literature [28] that the faults crossed by the pipeline along the project are basically in a range from 40 degrees to 90 degrees. Therefore, this study selects the strike-slip reverse faults with fault angles equal to 45 degrees, 60 degrees, 75 degrees, and 90 degrees. The variations in the axial strain and the von Mises stress of the pipeline under different fault angles are shown in Figure 9.
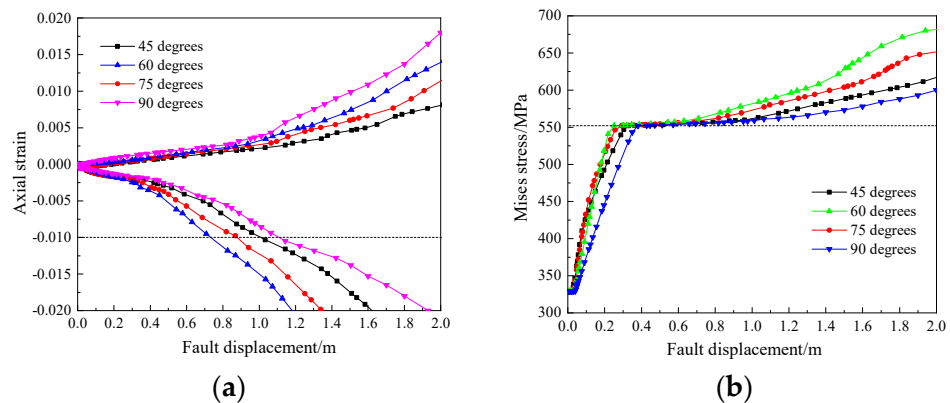
Figure 9. The response of pipeline under different fault angles: (**a**) Axial strain; (**b**) von Mises stress.

As can be seen from Figure 9a, the maximum axial tensile strain and compressive strain of the pipeline rise with the increasing fault displacement. The axial tensile strain

increases more slowly under different fault angles, and the growth rate is as follows, 90 degrees > 60 degrees > 75 degrees > 45 degrees. Before the fault displacement reaches 2 m, the pipeline does not reach the tensile damage standard under all fault angles. The changing trend of the axial compressive strain is different, it is fastest at a fault angle of 60 degrees and reaches the shell buckling damage criterion first.

As can be seen from Figure 9b, the evolution of the maximum Mises stress with the increase in fault displacement is similar to that of the compressive strain. The maximum von Mises stress grows the fastest under the fault at 60 degrees, and the growth rate is as follows, 60 degrees > 75 degrees > 45 degrees > 90 degrees. The growth rate of the von Mises stress remains unchanged in the four cases after the pipe yields, and the differences under the four fault angles are not significant. From the comprehensive stress and strain analysis, it can be determined that the risk of pipe failure is the highest under a fault angle of 60 degrees.

4.3. The Influence of Pipeline Internal Pressure

The internal pressure during the operation of long-distance buried pipelines has a significant impact on the economy and safety of pipelines. With the progress of science and technology, the performance of the steel used in pipelines is constantly improving, and the operating internal pressure that pipelines can withstand is also constantly improving. Most gas pipelines were built between the internal pressure of 3 and 10 MPa, while some pipelines have a higher internal pressure, such as the Second West–East Gas Pipeline Project (China), for which the internal design pressure can reach up to 12 MPa [28].

In this section, the internal pressures are taken to be 0 MPa, 3 MPa, 6 MPa, 9 MPa, and 12 MPa, and the corresponding critical axial compressive strains are calculated to be 0.0065, 0.007, 0.0085, 0.01, and 0.01, respectively (dashed line in Figure 10a). The variation in the axial strain and the von Mises stress of the pipeline under different internal pressures are plotted in Figure 10.
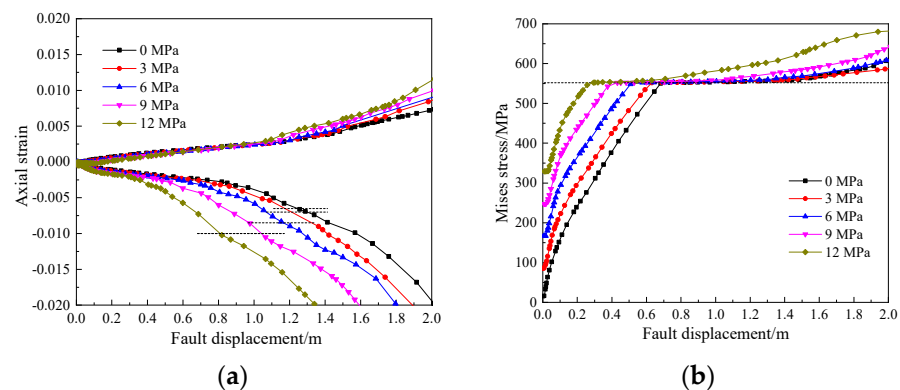
Figure 10. The response of pipeline under different internal pressures: (**a**) Axial strain; (**b**) von Mises stress.

As the displacement of the fault increases, the maximum axial tensile strain and compressive strain of the pipeline also increase. The growth rate with internal pressure is as follows, 0 MPa < 3 MPa < 6 MPa < 9 MPa. For the maximum axial tensile strains, the variation between the different internal pressures is not obvious, and ε_{tmax} is less than ε_t^{crit} under the five internal pressures when the fault displacement reaches 2 m. For the maximum axial compressive strains, the growth rate is more significantly increased with the increase in the internal pressures. With the increase in the internal pressure, the growth rate of ε_{cmax} rises more significantly, and the maximum axial compressive strain of the pipeline under the five types of internal pressures has been up to the shell buckling damage condition before the fault displacement reaches 2 m, as seen in Figure 10a.

From the comparative analysis of ε_{tmax} and ε_{cmax}, it can be seen that the existence of internal pressure in pipelines can partly offset the tensile effect caused by fault displacement,

and delays the growth of ε_{tmax}. However, the compression effect caused by pipeline internal pressure and fault dislocation superimposed on each other accelerates the growth rate of ε_{cmax}.

From Figure 10b, it can be seen that the maximum von Mises stress of the pipeline increases gradually with the increase in the internal pressure. Before reaching the yield strength, the stresses under five types of internal pressures increase relatively fast. The initial maximum von Mises stress of the pipeline is significantly different due to the existence of the internal pressure. The initial maximum von Mises stress of the pipeline without internal pressure is almost 0, while, when the internal pressure is 12 MPa, the initial maximum von Mises stress is as high as 330 MPa, which is equivalent to the maximum von Mises stress of the pipe without internal pressure when the fault displacement is 0.33 m.

Figure 11 depicts the deformation of the pipe for both cases, with and without internal pressure. When the internal pressure is 0 MPa, after the pipe is damaged by shell buckling, the location of the maximum axial compressive strain and the nearby wall will appear to be inwardly concave as the fault displacement continues to increase.

(a)   **(b)**
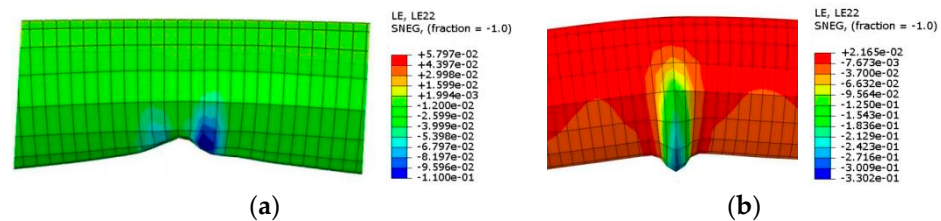
Figure 11. Deformation of pipelines under different internal pressures: (**a**) Internal pressure is 0; (**b**) internal pressure is 12 MPa.

In the presence of internal pressure, the pipe will eventually appear to be outwardly convex under the compressive effect after the pipe is damaged by shell buckling as the fault displacement increases. The maximum axial compressive displacement increases, the location of the strain and the nearby pipe wall in the compression will eventually appear to the outwardly convex. Furthermore, with the increase in the internal pressure, the pipe will appear more and more early convex, the pipe's convex degree will eventually be larger and larger. This behavior reflects that the existence of internal pressure in the pipeline can enhance the pipeline's deformation resistance ability. However, it should also be noted that an excessive internal pressure may make the pipeline more prone to damage under the action of fault displacement. Therefore, an appropriate operating internal pressure should be applied to pipelines according to actual requirements, in order to ensure transportation efficiency and fully maximize the pipe performance.

4.4. Influence of Pipe Wall Thickness

Here, to investigate the influence of wall thickness on the performance of pipes, four kinds of wall thicknesses are selected, 15.3 mm, 18.4 mm, 22.0 mm, and 26.4 mm, and the corresponding critical axial compressive strains are 0.0073, 0.0085, 0.01, and 0.0118, respectively (dashed line in Figure 12a). The variations in the axial strain and the von Mises stress of the pipeline under different pipe wall thickness are given in Figure 12.

As can be seen from Figure 12a, the critical fault displacements necessary for the pipe to reach tensile damage and shell buckling damage differ greatly under the four kinds of thicknesses. The overall trend can be described as, the thinner the wall is, the earlier the damage occurs in the pipe. When the wall thickness of the pipe is 15.3 mm, the growth rate of the tensile strain is significantly higher than for other thicknesses, and tensile damage occurs first when the fault displacement is 1.6 m. As the fault displacement increases, the tensile strain of the other wall thicknesses does not reach the critical condition of tensile damage before the fault displacement of 2 m.
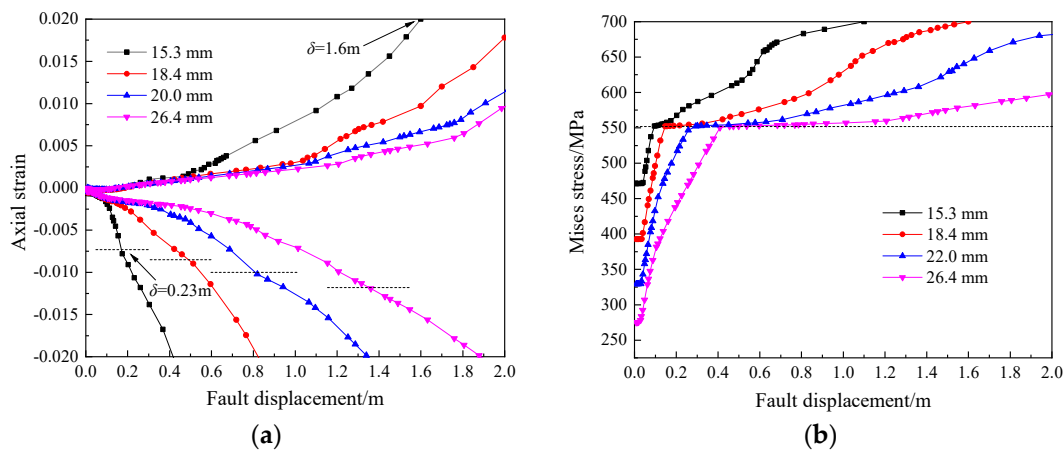
Figure 12. The response of pipeline under different wall thicknesses: (**a**) Axial strain; (**b**) von Mises stress.

The variation in the compressive strain between different wall thicknesses is even more obvious, and the pipeline with a wall thickness of 15.3 mm has already undergone shell buckling failure when the fault displacement is only 0.23 m. This shows that, when the wall thickness of the pipe is too small and there is a large pressure inside the pipe (12 MPa), the pipe may be in a very fragile state. The pipe will undergo shell buckling damage under a very small fault displacement, and the damage will develop very rapidly, making the pipeline experience large deformation.

In Figure 12b, it can be seen that the initial von Mises stress is as high as 471 MPa under an internal pressure of 12 MPa and wall thickness of 15.3 mm. The von Mises stress rises rapidly with the increase in fault displacement, and the yield strength of the pipe has been reached when the fault displacement is 0.096 m. After the von Mises stress of the pipe exceeds the yield strength, the growth rate of the von Mises stress with the fault displacement decreases with the increase in the wall thickness. When the wall thickness increases to 26.4 mm, the von Mises stress hardly increases up to 0.8 m of fault displacement change.

The deformation of pipelines also requires special attention. The deformation of the pipe with a wall thickness of 15.3 mm at fault displacements of 0.52 m, 0.62 m, and 0.72 m is shown in Figure 13. It can be seen that the pipe deformation changes considerably for every 0.1 m increase in fault displacement after shell buckling damage occurs in the pipe.
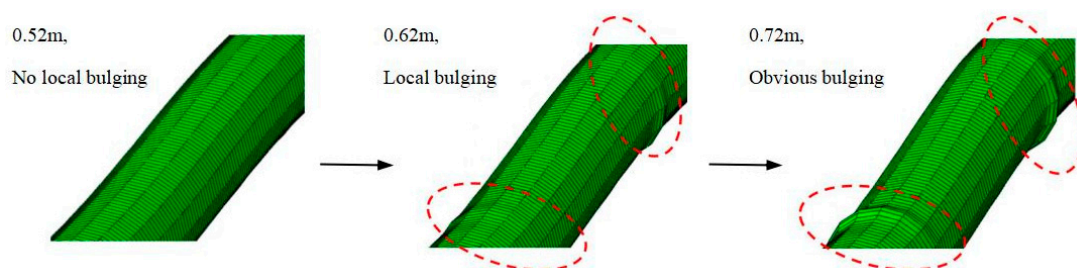
Figure 13. Development of pipe bulging as the displacement of faults increases.

The deformation of the pipe under four wall thicknesses is given in Figure 14, where the dashed line represents the location of the fault plane, and the length marked in the figure is the distance between the positions of the maximum axial compressive strain on both sides of the fault. It can be seen that, the smaller the wall thickness of the pipeline, the more obvious the deformation of the pipeline is under the same fault displacement, and the farther apart the maximum axial compressive strain on both sides of the fault is located. The main reason for this situation is that, during the fault displacement process,

the soil stiffness is relatively small compared to the pipe material, and the soil on both sides is equivalent to applying a flexible compression shear effect on the pipe. The smaller the wall thickness of the pipeline, the easier it is to damage, so the location of the damage is closer to the "shear plane" of the fault displacement surface.
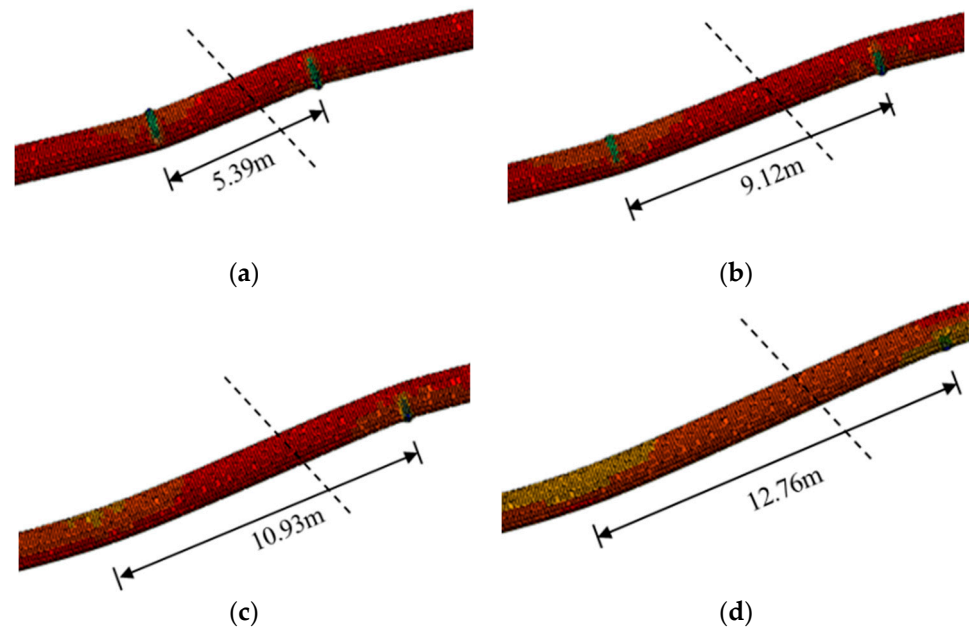
Figure 14. Deformation diagram of pipes under different kinds of wall thicknesses: (**a**) 15.33 mm; (**b**) 18.4 mm; (**c**) 22.0 mm; (**d**) 26.4 mm.

In summary, the wall thickness has a significant impact on the performance of buried pipelines. Generally speaking, the thicker the pipe wall, the safer the pipeline, but the amount of steel used will also increase accordingly. Therefore, it is recommended to choose an appropriate diameter to thickness ratio to balance economy and safety.

5. Conclusions

Based on advanced finite element simulation tools, a model of an interacting soil–pipeline system is established, and the mechanical behavior of buried steel pipelines crossing an active strike-slip fault was investigated, considering buried steel pipelines crossing the fault plane at various angles. Furthermore, this paper examines the mechanical behavior of buried steel pipelines under different fault types, their internal pressure, and their wall thickness.

(1) Among the three common damage modes, beam buckling damage is less threatening to the buried pipeline. The results show that beam buckling damage will not occur in the buried pipeline at the 1.5 m burial depth taken in this study. Shell buckling damage occurs at a small fault displacement (0.82 m), and the axial compressive strain of the pipeline develops rapidly with the increase in the fault displacement, which leads to outward bulging of the pipeline and even rupture. Although tensile failure may also occur, its critical failure displacement of 2.72 m is more than three times that of shell buckling failure, and the occurrence of shell buckling failure will accelerate the development of the maximum axial tensile strain of the pipeline;

(2) Compared to a single type of fault action, combined fault action has a more significant impact on buried pipelines, and the stress and strain of pipelines increase more rapidly when reverse faults exist. Under the action of strike-slip reverse faults, the threat is greater when the fault dip angle is 60 degrees;

(3) The internal pressure of a pipeline can, to some extent, enhance its ability to resist deformation, but excessive internal pressure can accelerate the development of stress

and strain in the pipeline, accelerating its failure process. After shell buckling failure occurs, a pipeline without internal pressure will have local inward depressions of the pipe wall, while a pipeline with high internal pressure will have local outward protrusions of the pipe wall;

(4) As the wall thickness decreases, the critical displacement necessary for pipeline failure gradually decreases, and the ability of pipelines to resist deformation significantly decreases. The point of pipeline wall failure will be closer to the fault displacement surface. If the wall thickness of the pipeline is too small, it may cause the entire pipeline to be in a fragile and easily damaged state under internal pressure.

Author Contributions: Conceptualization, R.Z. and S.L.; methodology, R.Z.; software, C.W. and S.L.; validation, S.L.; formal analysis, R.Z.; investigation, J.Z.; resources, W.L.; data curation, C.W.; writing—original draft preparation, R.Z.; writing—review and editing, R.Z.; supervision, R.Z. All authors have read and agreed to the published version of the manuscript.

Institutional Review Board Statement: Not applicable.

Informed Consent Statement: Not applicable.

Data Availability Statement: Not applicable.

Conflicts of Interest: The authors declare no conflict of interest.

References

1. MaCaffrey, M.A.; O'Rourke, T.D. Buried pipeline response to reverse faulting during the 1971 San Fernando Earthquake. *ASME PVP Conf.* **1983**, *77*, 151–159.
2. Nakata, T.; Hasuda, K. Active fault I 1995 Hyogoken Nanbu earthquake. *Kagaku* **1995**, *65*, 127–142.
3. *Kocaeli, Turkey Earthquake of August 17*; EERI Special Earthquake Report; Earthquake Engineering Research Institute: Oakland, CA, USA, 1999.
4. Takada, S.; Nakayama, M.; Ueno, J.; Tajima, C. *Report on Taiwan Earthquake*; RCUSS, Earthquake Laboratory of Kobe University: Kobe, Japan, 1999; pp. 2–9.
5. Shen, M.-D.; Zhou, J.-S.; Liu, X.-Y. Brief analysis on environmental geology and engineering geology in west section of second west to east gas pipeline project. *Pet. Eng. Constr.* **2010**, *S1*, 6–11.
6. Newmark, N.M.; Hall, W.J. Pipeline design to resist large fault displacement. In Proceedings of the US National Conference on Earthquake Engineering, Ann Arbor, MI, USA, 18–20 June 1975; pp. 416–425.
7. Guo, E.-D.; Feng, Q.-M. Aseismic analysis method for buried steel pipe crossing fault. *Earthq. Eng. Eng. Vib.* **1999**, *19*, 43–47.
8. Mitsuya, M.; Sakanoue, T.; Motohashi, H. Beam-Mode buckling of buried pipeline subjected to seismic ground motion. *ASME J. Pressure Vessel Technol.* **2013**, *135*, 021801. [CrossRef]
9. Zhang, L.-S.; Zhao, X.-B.; Yan, X.-Z.; Yang, X.-J. A new finite element model of buried steel pipelines crossing strike-slip faults considering equivalent boundary springs. *Eng. Struct.* **2016**, *123*, 30–44. [CrossRef]
10. Banushi, G.; Squeglia, N.; Thiele, K. Innovative analysis of a buried operating pipeline subjected to strike-slip fault displacement. *Soil Dyn. Earthq. Eng.* **2018**, *107*, 234–249. [CrossRef]
11. Shakib, H.; Zia-Tohidi, R. Response of steel buried pipelines to three-dimensional fault movements by considering material and geometrical non-linearities. In Proceedings of the 13th World Conference on Earthquake Engineering, Vancouver, BC, Canada, 1–6 August 2004.
12. Vazouras, P.; Karamanos, S.A.; Dakoulas, P. Finite element analysis of buried steel pipelines under strike-slip fault displacements. *Soil Dyn. Earthq. Eng.* **2010**, *30*, 1361–1376. [CrossRef]
13. Vazouras, P.; Karamanos, S.A.; Dakoulas, P. Mechanical behavior of buried steel pipes crossing active strike-slip faults. *Soil Dyn. Earthq. Eng.* **2012**, *41*, 164–180. [CrossRef]
14. Vazouras, P.; Dakoulas, P.; Karamanos, S.A. Pipe–soil interaction and pipeline performance under strike–slip fault movements. *Soil Dyn. Earthq. Eng.* **2015**, *72*, 48–65. [CrossRef]
15. Gu, X.; Zhang, H. Research on aseismatic measures of gas pipeline crossing a fault for strain-based design. In Proceedings of the ASME 2009 Pressure Vessels and Piping Division Conference, Prague, Czech Republic, 26–30 July 2009.
16. Cheng, X.-D.; Pang, M.-W.; Xu, L.; Su, Q.-Z.; Xiang, E.-Z.; Hu, W.-J. Seismic response analysis of buried pipelines crossing oblique slip faults based on a strain design. *Nat. Gas. Ind.* **2016**, *36*, 110–117.
17. Cheng, X.-D.; Ma, C.; Huang, R.-K.; Huang, S.-N.; Yang, W.-D. Failure mode analysis of X80 buried steel pipeline under oblique-reverse fault. *Soil Dyn. Earthq. Eng.* **2019**, *125*, 105723. [CrossRef]

18. Ma, C.; Cheng, X.-D.; Xu, T.-Z.; Xu, L.-Y.; Wang, Y.; An, K.; Hu, W.-J. Research on local buckling failure range of X80 buried steel pipeline under oblique-reverse fault. *Soil Dyn. Earthq. Eng.* **2023**, *164*, 107592. [CrossRef]

19. Ha, D.; Abdoun, T.H.; O' Rourke, M.J.; Symans, M.D.; O' Rourke, T.D.; Palmer, M.C.; Stewart, H.E. Buried high-density polyethylene pipelines subjected to normal and strike-slip faulting-a centrifuge investigation. *Can. Geot. J.* **2008**, *45*, 1733–1742. [CrossRef]

20. Ha, D.; Abdoun, T.H.; O' Rourke, M.J.; Symans, M.D.; O' Rourke, T.D.; Palmer, M.C.; Stewart, H.E. Centrifuge modelling of earthquake effects on buried high-density polyethylene (HDPE) pipelines crossing fault zones. *ASCE J. Geotech. Geoenviron. Eng.* **2008**, *134*, 1501–1515. [CrossRef]

21. Abdoun, T.H.; Ha, D.; O'Rourke, M.J.; Symans, M.D.; O' Rourke, T.D.; Palmer, M.C.; Stewart, H.E. Factors influencing the behavior of buried pipelines subjected to earthquake faulting. *Soil Dyn. Earthq. Eng.* **2009**, *29*, 415–427. [CrossRef]

22. Zhang, R.-L.; Jiang, C.; Li, S.; Zhang, Z.-T. Numerical simulation of response of steel buried pipeline across fault. *World. Earthq. Eng.* **2023**, *39*, 46–52.

23. *ABAQUS User's Guide*; Version 6.13; Simulia: Providence, RI, USA, 2013.

24. Ministry of Housing and Urban-Rural Development of the People's Republic of China. *GB/T 50470-2017 Seismic Technical Code for Oil and Gas Transmission Pipeline Engineering*; China Planning Press: Beijing, China, 2017.

25. Kaya, E.S.; Uckan, E.; O'Rourke, M.J.; Karamanos, S.A.; Akbas, B.; Cakir, F.; Cheng, Y. Failure analysis of a welded steel pipe at Kullar fault crossing. *Eng. Fail. Anal.* **2017**, *71*, 43–62. [CrossRef]

26. Ma, C. Study on the Failure Mode of Buried X80 Steel Pipe under the Action of Oblique Reverse Fault. Master's Thesis, University of Petroleum (East China), Qingdao, China, 2020.

27. Qi, X.-B. Research on Mechanical Performance of Buried Steel Gas Transmission Pipeline Crossing Strike-Slip Fault. Master's Thesis, Northeast Petroleum University, Daqing, China, 2022.

28. Yu, Z.-F.; Wang, G.-L.; Shi, H. *Q/SY GJX 0136-2008 Guideline for Strain-Based Design in Seismic Area and Active Fault Crossing of the Second West-East Natural Gas Transportation Pipeline Project*; Petroleum Industry Press: Beijing, China, 2008.

29. Meyersohn, W.D.; O'Rourke, T.D. *Pipeline Buckling Caused by Compressive Ground Failure During Earthquakes*; National Center for Earthquake Engineering Research: New York, NY, USA, 1991.

30. *CSA Z662-2015*; Oil and Gas Pipeline Systems. Canadian Standard Association: Toronto, ON, Canada, 2015.

31. *DNV-OS-F101*; Det Norske Veritas. Offshore Standard-Submarine Pipeline Systems: Høvik, Norway, 2007.